Electronic supplement to "Bedload transport: a walk between randomness and determinism"

Christophe Ancey

September 2019

1 Video 1: sediment waves

1.1 Caption

The video "TimelapseRun14_20161130T181447" shows the timelapse animation created by Blaise Dhont from a series of images taken at the sidewall of the Armfield flume (Dhont, 2017). The video shows 24 hr of the entire sequence (the time is indicated at the right bottom corner). The bottom pane shows the time series $Q_s(t)$, which ranged from 0 to 19.3 g during this period of time. The green bands that appear intermittently are due to the laser scanning used for measuring bed topography (Dhont, 2017).

1.2 Experimental protocol

During his PhD thesis, Dhont used a 19-m long 60-cm wide flume, whose bottom was inclined at 1.6% to the horizontal (Dhont, 2017; Dhont and Ancey, 2018). At the inlet, the water discharge was $Q_w = 15\ \mathrm{l\,s^{-1}}$ (uncertainty 0.01 $\mathrm{l\,s^{-1}}$), while the feed rate was $Q_{in} = 2.5$ $\mathrm{g\,s^{-1}}$ (relative uncertainty 10%). The experiment was run for 250 h. The video shows how the granular bed evolved with time, and the time-averaged transport rate Q_s recorded at the flume outlet. Although the feed rare was constant, the bedload transport rate fluctuated widely, with peak values exceeding 40 g/s. The mean Froude number was close to unity, as is often the case for this kind of conditions (Grant, 1997). The flow depth h was 4 cm on average, but much larger in the pools ($h \sim 10$ cm). The mean flow velocity was close to 1 m $\mathrm{s^{-1}}$. By and large, the Shields number ranged from 0.05 to 0.1, which corresponded to incipient or weak particle transport.

The bed was composed of well-sorted natural gravel with a mean diameter 5.5 mm (diameter standard deviation: 1.2 mm). Initially the bed was flat and of uniform thickness (32 cm). It was maintained in place by a drilled plate fixed to the flume outlet. In the absence of holes, the hyporheic flow would have come up near the flume outlet, and disturb sediment transport by favoring particle entrainment. As planar beds are unstable, bedforms (here, pools and alternate bars) developed along the bed, causing a slope adjustment over a transient phase of duration $t_a \sim 678$ min. Initially the bed slope was set 1.6%. The time-averaged bed slope (over the run duration) was 1.48%, while its standard deviation was 0.07%.

The water discharge was controlled by a recirculating pump and monitored using an EH Promag 50 flow meter (Reinach, Switzerland). A hopper stored the gravel, and released a fixed amount of it per unit time, which was then taken to the flume inlet by a conveyor belt (manufactured by Electra, France). The feed rate was mainly controlled by the hopper's orifice diameter and belt velocity, but also depended on other factors (e.g., water content and grain diameter). A Galton board placed at the flume inlet spread the incoming material nonuniformly, but fully across the width (most particles fell near the flume centerline). See movie 1.

The bedload transport rate was measured using six accelerometers (Freescale Semiconductor MMA7361LC) operated at a sampling frequency of 10 kHz. The accelerometers were mounted on six vertical plates placed 5 cm away from the flume outlet. When leaving the flume, particles hit the plates, and the resulting vibrations were recorded by the accelerometers (Mettra, 2014). Using a peak-over-threshold method, we were able to determine the number of particles hitting the plates per unit time (Dhont et al., 2017). The signal recorded saturated when the plates were not stroke by isolated grains, but by clusters. This occurred for bedload transport rates q_s in excess of 3.1 g s^{-1}. The accelerometers were thus calibrated to get around this issue and provide the bedload transport rate over the full range of transport rates (Dhont et al., 2017). Compared to other related techniques, vertical impact plates had the advantage of high accuracy in the measurement of Q_s as the relative uncertainty did not exceed 4%. A basket was also placed underneath the flume outlet to collect the sediment. Weighting the collected material provided another way of estimating the time-averaged transport rates. The instantaneous transport rates were averaged over a time step $\Delta t = 1$ min. All the analysis was based on these time-averaged values. The bedload transport rate averaged over the whole run duration was $\bar{Q}_s = 4.82$ g s^{-1}. While this value did not match the feed rate Q_{in} exactly, we did not observe neither noticeable aggradation nor degradation in the long run, and as time variations in the feed rate Q_{in} could reach 10%, we think that the two rates were reasonably close to be considered equal.

Every 10 min, we measured flow depth and bed topography using ultrasonic probes (UNAM 30I6103 manufactured by Baumer Electric) and image processing (Visconti et al., 2012), respectively. To that end, a laser (BES536-L supplied by Apinex, wavelength 532 nm, 50 mW) mounted on an automated mobile cart projected a line across the width through the water (Dhont, 2017). A color camera (a Basler acA2000-165uc operated at 5 Hz) tracked the line deformations. After postprocessing (correction of distortion and refraction), we could relate line deformation and bed elevation, and thereby obtain the bed elevation map in the form of

a 60×281 matrix (representing a 60×1400-cm^2 area). The absolute uncertainties on flow depth and bed elevation were 0.5 mm and 1 cm, respectively. Webcameras were also placed along the flume sidewall and took images from the left side. Time-lapses videos were created by stitching the pictures taken by these cameras.

1.3 Interpretation

At the timescale of observation (1 second of video represents about 2100 s during the run), particles moving individually are difficult to see clearly, but carefully looking at the video shows that many isolated particles move along the bed. What jumps out at the careful observer is the propagation of coherent sediment waves. One is visible at time $t = 8$ s (run time 1 Dec. 2016, 00:04) on the left. At time $t = 16$ s (run time 1 Dec. 2016, 04:20), erosion is visible in the pool on the right. Suddently, the water's erosive action is more pronounced, and in a few seconds (about 2h30 in the experiment), the bedform has been destroyed.

2 Video 2: particle motion

2.1 Caption

The videos movieJoris1 and movieJoris2 show moving particles Using a particle tracking algorithm, Joris Heyman managed to focus on the moving particle, while computing its velocity, acceleration and rotation (velocity is given in the bottom panel, while the acceleration is plotted in the form of a vector in the upper right corner). Time since initial entrainment is indicated in the upper left corner (Heyman et al., 2016). The second video movieJoris2 shows that particles can be entrained not only as a result of the bottom drag exerted by the flow, but also because of particle collisions.

2.2 Experimental protocol

During his thesis, Joris Heyman used a 2.5-m long 3.5-cm wide flume tilted at about 4% to the horizontal (Heyman, 2014; Heyman et al., 2014, 2016). As the flume was narrow, he was able to track particles by tacking images from the size. The experimental techniques are presented in his papers (Heyman, 2014; Heyman et al., 2014, 2016). In the videos, the Froude number was close to 1.2, while the Shields number was about 0.1.

3 Further definitions of the bedload transport rate

The first step is to define what bedload transport means. It is usual to distinguish between *suspended sediment* and *bedload*. Suspended particles are those maintained in suspension

in the stream by turbulence, with no contact with the bed. By contrast, bedload involves particles moving along the bed, with permanent (by rolling) or intermittent (by saltating) contacts along the bed. This partitioning may look simple on paper, but taking a closer look at experiments or implementing it into an image processing algorithm raises difficulties. Some issues like differentiating between jiggled resting and rolling states lead to marginal errors, but others are more difficult to discern. At low sediment transport rate, many particles move individually, but some move collectively, forming a coherent ensemble of particles. It is tempting to call this ensemble a *sediment wave*, but as the expression has been used in various contexts, it may be ambiguous (Lisle, 2004). As shown in the video, these sediment waves may move at a lower velocity than isolated particles, and thus they may be viewed as the bed's slow creeping motion driven by sediment transport. They may also move as granular flows (en masse), with a thickness spanning several particle diameters and a velocity that matches that of isolated particles. These flows occur frequently in the form of avalanches from the banks or dune's lee side, but they are also observed when bedforms suddenly release fixed volumes of sediment (Dhont and Ancey, 2018). At high sediment transport rate, many particles move collectively. They form a shallow layer of rolling and saltating particles, which is closer to a granular gas than a coherent dense granular carpet. Differentiating the various forms of motion has proven to be difficult because of the overlapping of time and length scales featuring each of them.

The second step is to define the bedload transport rate Q_s. A number of expressions have been proposed to serve different purposes depending on the experimental constraints (Ancey, 2010; Furbish et al., 2012; Campagnol et al., 2012; Ballio et al., 2014, 2018, 2019). For a fluid mechanician, it seems natural to define the flux of particles Q_s across a control surface S

$$Q_s(t) = \int_S H(\boldsymbol{x}) \boldsymbol{u}_p \cdot \boldsymbol{n} \mathrm{d}S, \tag{1}$$

where $\boldsymbol{n}$ denotes the unit normal to control surface and H is the phase-indicating function: $H(\boldsymbol{x}) = 1$ when $\boldsymbol{x}$ lies inside a particle, and $H(\boldsymbol{x}) = 0$ when $\boldsymbol{x}$ lies in the carrying fluid. This definition turns out to be difficult to apply experimentally or theoretically. In practice, it is possible to count the number of particles crossing a surface by using, for instance, image processing or geophones, but this is done by counting the number of particles that have crossed the surface over a period of time δt, not by measuring the instantaneous flux. Theoretically, as bedload involves discrete particles, it is difficult to apply Eq. (1), which is better suited to continua. Again, an expedient is to count the number N of particles that cross the control surface over the time length δt:

$$\bar{Q}_s(t) = \frac{N \varpi_i}{\delta t}. \tag{2}$$

In both cases arises the problem of determining how sensitive the transport rate Q_s is to changes in δt. Naively we may think by evoking the law of large numbers that the measurement error decreases with increasing δt, and as is often stated in experimental papers, we just have to wait sufficiently long for obtaining a reliable measurement of the time-average transport rate. The convergence may be quite slow, and it is difficult to predetermine the right sampling time.

If we put the emphasis on the discrete of bedload transport, then it is more natural to view it as a granular gas and use tools inspired from kinetic theory (Lhuillier, 1992; Drew and Passman, 1999). We define the solid discharge as the ensemble average of the particle flux

$$\langle Q_s \rangle = \int_S \int_{\mathbb{R}^2} P[\boldsymbol{u}_p \mid \boldsymbol{x},\, t]\; \boldsymbol{u}_p \cdot \boldsymbol{k}\; |d\boldsymbol{x}| d\boldsymbol{u}_p. \tag{3}$$

where $P[\boldsymbol{u}_p \mid \boldsymbol{x},\, t]$ is the probability that a particle crosses the control surface S at position $\boldsymbol{x}$ and time t with velocity $\boldsymbol{u}_p$. Note that $\boldsymbol{u}_p$ is a velocity field, which is $\boldsymbol{u}_p(\boldsymbol{x}, t) = \boldsymbol{x}_G + \boldsymbol{\Omega} \times (\boldsymbol{x} - \boldsymbol{x}_G)$ where $\boldsymbol{x}$ lies inside a particle with velocity $\boldsymbol{u}_G$ at the center of mass $\boldsymbol{x}_G$ and rotational velocity $\boldsymbol{\Omega}$; where $\boldsymbol{x}$ lies in the fluid phase, this field is zero. Interesting from the theoretical standpoint, Eq. (3) is of limited practical interest in this form, but a more handy form can be derived. Under steady state conditions, ensemble averages can be swapped with volume averages. Equation (3) takes the following form

$$\langle Q_s \rangle = \int_S c(y) u_p(y) \mathrm{d}y, \tag{4}$$

where we exploit the correspondence between concentration and probability of finding one particle at a given place. This form was used notably by Wiberg and Smith (1989), Charru et al. (2004) and Ancey et al. (2008), and related forms by Yalin (1963), Bridge and Dominic (1984), Kovacs and Parker (1994), and García (2007). To evaluate the particle concentration, we can substitute integration over a control surface with a volume integration

$$\bar{Q}_s = \frac{S}{V} \sum_{i=1}^{N} \varpi_i u_{p,i} = \frac{N \varpi_p \bar{u}_p}{L} = \gamma \bar{u}_p \tag{5}$$

where ϖ_p is the mean particle volume and integration has been performed over the control volume ($\mathcal{V} = L \times S$) of length L, which is sufficiently long to contain a number of particles, but is short enough compared to the scale of variation of q_s on the macroscopic scale, $u_{p,i} = \boldsymbol{u}_p \cdot \boldsymbol{k}$ denote the streamwise velocity component of particle i, and $\bar{u}_p$ is the volume-averaged particle velocity. A related form is $\gamma \bar{u}_p$ (Furbish et al., 2012), $\gamma = N\varpi/L$ denotes the *particle activity*, that is, the volume of moving particles per unit streambed width. Equations (2) and (5) are related if we set $L = \bar{u}_p \delta t$.

Another perspective was provided by Simons et al. (1965), who emphasized the part played by bedforms in the bedload transport rate. The equation proposed by Simons et al. (1965) (see the review paper) has been extended to reflect the multiscale nature of bedform (Nikora, 1984; Guala et al., 2014)

$$q_s = (1 - \zeta) \int_{k_{min}}^{k_{max}} A(k) C(k) \mathrm{d}k, \tag{6}$$

which can be interpreted as follows: a bedform is featured by its wave number $k = 2\pi/\lambda$ (with λ the wave length), and this bedform of area $A(k)$ moving at a velocity $C(k)$ contributes to the bedload transport rate.

In addition to the approaches viewing bedload transport as a continuum lie approaches that focus on the 'fate' of individual particles. To monitor how particles spread along a flume,

Einstein (1937) painted particles in different colors. Use of tracers has been quite common since then, especially in field surveys. Einstein (1950) considered that bedload transport results from the mismatch between the entrainment and deposition rates, E and D, respectively. This amounts to writing that on a small interval Δx, the bedload transport increment is $\delta q_s = (E - D)\Delta x$. Under bed equilibrium conditions (when $E = D$), Einstein (1950) defined the sediment transport rate as

$$q_s = E\bar{\ell}, \tag{7}$$

where $\bar{\ell}$ is the mean length travelled by individual particles during each leap. Several field measurement campaigns used Einstein-like definitions to monitor bedload transport under incipient-motion conditions (Drake et al., 1988; Habersack, 2001; Wilcock, 1997; Pryce and Ashmore, 2003). Laboratory experiments as well as theoretical analyses made extensive use of this definition (Fernandez Luque and van Beek, 1976; Seminara et al., 2002). From the observation that particles can be moving, lying at rest on the bed surface, or buried in the bed, we can define a virtual velocity, which is the time-averaged velocity U_p (called *virtual particle velocity*) of an individual particle. Only the upper bed layer participates in bedload transport and is therefore termed the *active layer* (Church and Haschenburger, 2017); the thickness of this layer is L_a and represents the depth down to which the bed is continuously reworked by fill and scour. Mass conservation then implies that

$$q_s = U_p L_a. \tag{8}$$

The use of this equation has been documented for both natural rivers (Ferguson et al., 2002; Ferguson and Hoey, 2002; DeVries, 2002; Cudden and Hoey, 2003) and flume experiments (Wong et al., 2007; Ganti et al., 2010).

4 The Navisence River

4.1 Location and monitoring station

In the late 2000s, within a joint research project involving CREALP (Sion) and EPFL, we started to work on the Navisence River, a mountain stream in Canton du Valais (Switzerland). The watershed area is 47 km^2, elevation ranges from 1600 m to 4500 m). The glaciers cover 55% of the watershed surface, whereas forested areas do not exceed 5%. The Navisence River is gravel-bed river originating from the Weisshorn-glacier melt-water streams about 5 km upstream of the study area.

The area of interest is the alluvial plain called *Plat de la Lé*. It comprises:

- a multiple-thread river flowing over its alluvium (mean slope of 4.1%). This 5-km long reach is typical of gravel-bed braided rivers (see the picture on the cover page);
- the tributaries draining lateral hillslopes;
- the hydrogeological system feeding the Navisence River.

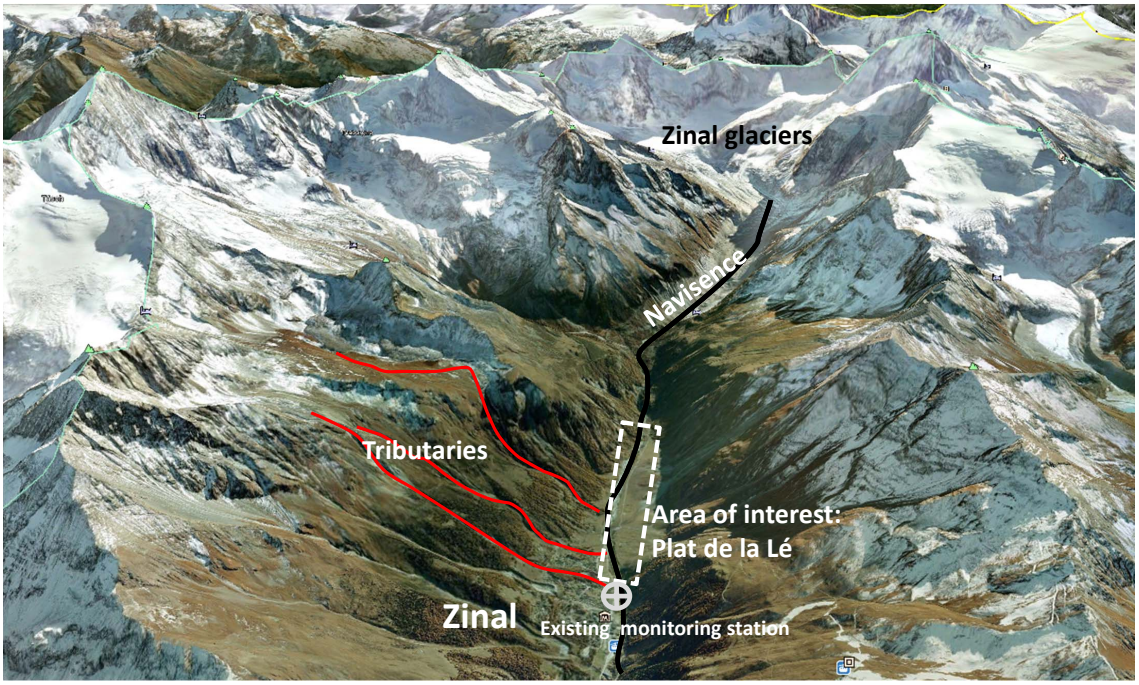

Figure 1: View of the Navisence Valley's upper part (Valais, Switzerland). Zinal (1600 m) is the village at the valley bottom. The valley is dominated by several summits over 4000 m and is drained by the Navisence River. A monitoring station has been in operation since 2011.

The focus has been on a 5-km long reach, whose average bed gradient is 4.1% (from 1750 m to 1550 m in altitude). This reach is split into two parts:

- The first part (upstream of the Zinal dwellings) is called *Plat de la Lé* (see Fig. 3). It is characterised by a milder slope (2.5%) and a wider floodplain (50 m). Pool-riffle and braiding channels are usually observed in this river section (see the cover page).
- The second part is steeper (up to 8%) and exhibits a step-pool morphology and a narrow single-thread channel incised in glacial deposits.

A monitoring station was built downstream of the Plat de la Lé by WSL in 2011 (see Fig. 4). The sediment transport rate is continuously recorded using 6 geophones (Wyss et al., 2016). Other parameters such as water discharge and temperature are measured at high temporal resolution. Since 2017, bed topography has been monitored (on the Plat de la Lé) using a drone. Images are processed using the PiX4D software.

The monitoring station was destroyed by a flood in August 2013 and another in July 2018. As a consequence, we have data from May 2011 to August 2013, from May 2014 to July 2018, and from May 2019 on. The station has been calibrated so that we can estimate the water discharge Q_w from the flow depth measurement. The calibration holds for $Q_w \leq 25$ m^3/s.

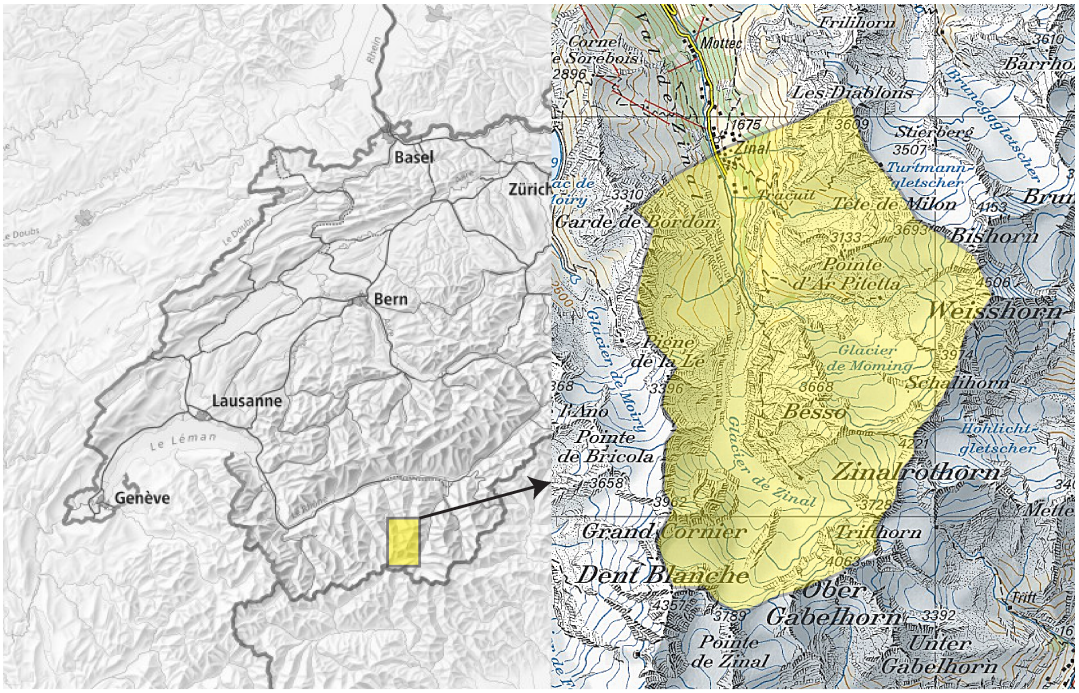

Figure 2: Location map of the site.

4.2 Data

The `DataNavisence.txt` file contains the following data: for each water discharge Q_w (in m^3/s, column 1) I provide the mean transport rate associated with this discharge Q_s (in m^3/s, column 2). I considered data from 2011 to 2017). Columns 3 to 5 provide the Q_s moments of order 2 to 4. Column 6 provides the Q_s quantile associated with the probability 0.10, columns 7 to 9 do the same for quantiles associated with probabilities 0.90, 0.025, and 0.975. Columns 10 and 11 provide the minimum and maximum values of àQ_s for each Q_w. The Mathematica notebook called `figure2.nb` used for creating Fig. 2 is also proposed.

Figure 3: View of the site. The picture shows the upper reach of the Navisence River above Zinal (Switzerland, Wallis) in the alluvial plain called “Plat de la Lé.”

Figure 4: Two views of the station: (a) from upstream. The two beams serve as bridge during the winter (back-country skiing track). The geophones are located underneath these beams. Eric Bardou and Blaise Dhont in October 2013 discussing the station's repair works. (b) View from the side. François Mettra calibrating the station in July 2011.

Table of Notation

Here I provide the list of variables used in the paper, their meaning, and physical units.

Roman symbols

Variable	Meaning
d	particle diameter [m]
D	particle diffusivity [$\mathrm{m\,s^{-2}}$]
D_*	fake diffusivity [$\mathrm{m\,s^{-2}}$]
D	deposition rate per unit area [$\mathrm{s^{-1}}$]
E	entrainment rate per unit area [$\mathrm{s^{-1}}$]
f	probability density function
F	exceedance probability
g	gravity acceleration $g = 9.81$ $\mathrm{m\,s^{-2}}$
h	flow depth [m]
i	bed slope
ℓ	correlation length [m]
$\bar{\ell}$	
N, n	number of moving particles within the window
P, p	probability density function
$\bar{q}_s$	time-averaged particle sediment rate [part. $\mathrm{s^{-1}}$]
q_s	instantaneous particle sediment rate [part. $\mathrm{s^{-1}}$]
Q_{in}	
Q_w	water discharge [$\mathrm{m^3\,s^{-1}}$]
q_w	water discharge per unit width [$\mathrm{m^2\,s^{-1}}$]
$R = \varrho_s/\varrho - 1$	density ratio
t	time [s]
$\bar{u}_p$	mean particle (advection) velocity in [$\mathrm{m\,s^{-1}}$]
$u_* = \sqrt{\tau_b/\varrho}$	friction velocity
u_c	critical velocity
v_s	settling velocity
x	streamwise coordinate [m]
y_b	bed elevation [m]

Greek and compound symbols

variable	meaning
δt	time increment [s]
Δx	space increment [m]
γ	particle activity [m]
λ	entrainment rate [s^{-1}]
μ	collective entrainment rate [s^{-1}]
ν	emigration rate [s^{-1}]
ϱ	sediment density [kg m^{-3}]
ϱ_s	sediment density [kg m^{-3}]
σ	deposition rate [s^{-1}]
ϖ_p	particle volume [m^3]
$\Theta = \frac{\tau_b}{\varrho R g d}$	Shields number
$\Phi = \frac{q_s}{d\sqrt{gRd}}$	dimensionless transport rate
$\Psi = (\varrho_s - \varrho) g d / (\varrho u_*^2) = \Theta^{-1}$	bedload intensity
τ_b	bottom shear stress [Pa]
τ_c	critical shear rate (incipient motion) [Pa]
ω	stream power per unit width [W m^{-1}]
θ	bed inclination
ζ	bed porosity

References

Ancey, C. (2010). Stochastic approximation of the Exner equation under lower-regime conditions. *J. Geophys. Res.*, 115:F00A11.

Ancey, C., Davison, A. C., Böhm, T., Jodeau, M., and Frey, P. (2008). Entrainment and motion of coarse particles in a shallow water stream down a steep slope. *J. Fluid Mech.*, 595:83–114.

Ballio, F., Nikora, V., and Coleman, S. (2014). On the definition of solid discharge in hydroenvironment research and applications. *J. Hydraul. Res.*, 52:173–184.

Ballio, F., Pokrajac, D., Radice, A., and Hosseini Sadabadi, S. A. (2018). Lagrangian and Eulerian description of bed-load transport. *J. Geophys. Res Earth Surf.*, 123:384–408.

Ballio, F., Radice, A., Fathel, S. L., and Furbisch, D. (2019). Experimental Censorship of Bed Load Particle Motions and Bias Correction of the Associated frequency distributions. *J. Geophys. Res Earth Surf.*, 124:116–136.

Bridge, J. and Dominic, D. (1984). Bed load grain velocities and sediment transport rates. *Water Resour. Res.*, 20:476–490.

Campagnol, J., Radice, A., and Ballio, F. (2012). Scale-based statistical analysis of sediment fluxes. *Acta Geophys.*, 60:1744–1777.

Charru, F., Mouilleron, H., and Eiff, O. (2004). Erosion and deposition of particles on a bed sheared by a viscous flow. *J. Fluid Mech.*, 519:55–80.

Church, M. and Haschenburger, J. K. (2017). What is the "active layer"? *Water Resour. Res.*, 53:5–10.

Cudden, J. and Hoey, T. B. (2003). The causes of bedload pulses in a gravel channel: The implications of bedload grain-size distributions. *Earth Surf. Process. Landforms*, 28:1411–1428.

DeVries, P. (2002). Bedload layer thickness and disturbance depth in gravel bed streams. *J. Hydraul. Eng.*, 128:983–991.

Dhont, B. (2017). *Sediment Pulses in a Gravel-Bed Flume with Alternate Bars*. PhD thesis, École Polytechnique Fédérale de Lausanne.

Dhont, B. and Ancey, C. (2018). Are bedload transport pulses in gravel-bed rivers created by bar migration or sediment waves. *Geophys. Res. Lett.*, 45:5501–5508.

Dhont, B., Rousseau, G., and Ancey, C. (2017). Continuous monitoring of bedload transport in a laboratory flume using an impact sensor. *J. Hydraul. Eng.*, 143:04017005.

Drake, T., Shreve, R., Dietrich, W., and Leopold, L. (1988). Bedload transport of fine gravel observed by motion-picture photography. *J. Fluid Mech.*, 192:193–217.

Drew, D. and Passman, S. (1999). *Theory of Multicomponent Fluids*. Springer, New York.

Einstein, H. (1937). *Der Geschiebetrieb als Wahrscheinlichkeitproblem (Bedload transport as a*

probability problem). (english translation by W. W. Sayre, in Sedimentation (Symposium to honor H. A. Einstein), edited by H. W. Shen, Fort Collins, Colorado, 1972, C1–C105, ETHZ.

Einstein, H. (1950). The bed-load function for sediment transportation in open channel flows. Technical Report Technical Report No. 1026, United States Department of Agriculture.

Ferguson, R., Bloomer, D., Hoey, T., and Werritty, A. (2002). Mobility of river tracer pebbles over different timescales. *Water Resour. Res.*, 38:10.1029/2001WR000254.

Ferguson, R. I. and Hoey, T. B. (2002). Long-term slowdown of river tracer pebbles: Generic models and implications for interpreting short-term tracer studies. *Water Resour. Res.*, 38:2001WR000637.

Fernandez Luque, R. and van Beek, R. (1976). Erosion and transport of bed-load sediment. *J. Hydraul. Res.*, 14:127–144.

Furbish, D., Haff, P., Roseberry, J., and Schmeeckle, M. (2012). A probabilistic description of the bed load sediment flux: 1. Theory. *J. Geophys. Res.*, 117:F03031.

Ganti, V., Meerschaert, M., Foufoula-Georgiou, E., Viparelli, E., and Parker, G. (2010). Normal and anomalous dispersion of gravel tracer particles in rivers. *J. Geophys. Res.*, 115:F00A12.

García, M., editor (2007). *Sedimentation Engineering*, volume 110. ASCE Manuals and Reports on Engineering Practice, Reston.

Grant, G. (1997). Critical flow constrains flow hydraulics in mobile-bed streams: a new hypothesis. *Water Resour. Res.*, 33:349–358.

Guala, M., Singh, A., BadHeartBull, N., and Foufoula-Georgiou, E. (2014). Spectral description of migrating bed forms and sediment transport. *J. Geophys. Res Earth Surf.*, 119:123–137.

Habersack, H. (2001). Radio-tracking gravel particles in a large braided river in New Zealand: a field test of the stochastic theory of bed load transport proposed by Einstein. *Hydrolog. Process.*, 15:377–391.

Heyman, J. (2014). *A study of the spatio-temporal behaviour of bed load transport rate fluctuations.* PhD thesis, École Polytechnique Fédérale de Lausanne.

Heyman, J., Bohorquez, P., and Ancey, C. (2016). Entrainment, motion, and deposition of coarse particles transported by water over a sloping mobile bed. *J. Geophys. Res Earth Surf.*, 121:1931–1952.

Heyman, J., Ma, H., Mettra, F., and Ancey, C. (2014). Spatial correlations in bed load transport: Evidence, importance, and modeling. *J. Geophys. Res Earth Surf.*, 119:1751–1767.

Kovacs, A. and Parker, G. (1994). A new vectorial bedload formulation and its application to the time evolution of straight rivers. *J. Fluid Mech.*, 267:153–183.

Lhuillier, D. (1992). Ensemble averaging in slightly non-uniform suspensions. *Eur. J. Mech. B. Fluids*, 6:649–661.

Lisle, T. E. (2004). Sediment wave. In Goudie, A., editor, *Encyclopedia of Geomorphology*, volume 2, page 938. Routledge, London.

Mettra, F. (2014). *Morphodynamic mechanisms in steep channels: from local processes to large-scale evolution.* PhD thesis, École Polytechnique Fédérale de Lausanne.

Nikora, V. (1984). *The structure of turbulent flow and statistical characterisation of dune-covered river beds (with examples of field studies in rivers Turunchuk, Rioni, and Tsheniscali).* PhD thesis.

Pryce, R. and Ashmore, P. (2003). The relation between particle path length distributions and channel morphology in gravel-bed streams: a synthesis. *Geomorphology*, 1353:1–21.

Seminara, G., Solari, L., and Parker, G. (2002). Bed load at low Shields stress on arbitrary sloping beds: failure of the Bagnold hypothesis. *Water Resour. Res.*, 38:1249.

Simons, D. B., Richardson, E. V., and Nordin, C. F. (1965). Bedload equation for ripples and dunes. Technical Report Professional Paper 462 H, U.S. Geological Survey.

Visconti, F., Stefanon, L., Camporeale, C., Susin, F., Ridolfi, L., and Lanzoni, S. (2012). Bed evolution measurement with flowing water in morphodynamics experiments. *Earth Surf. Process. Landforms*, 37:818–827.

Wiberg, P. and Smith, J. (1989). Model for calculating bedload transport of sediment. *J. Hydraul. Eng.*, 115:101–123.

Wilcock, P. (1997). Entrainment, displacement and transport of tracer gravels. *Earth Surf. Process. Landforms*, 22:1125–1138.

Wong, M., Parker, G., DeVries, P., Brown, T., and Burges, S. (2007). Experiments on dispersion of tracer stones under lower-regime plane-bed equilibrium bed load transport. *Water Resour. Res.*, 43:W03440.

Wyss, C. R., Rickenmann, D., Fritschi, B., Turowski, J. M., Weitbrecht, V., Travaglini, E., Bardou, E., and Boes, R. M. (2016). Laboratory flume experiments with the Swiss plate geophone bedload monitoring system. Part II: Application to field sites with direct bedload samples. *Water Resour. Res.*, 52:7760–7778.

Yalin, M. (1963). An expression for bed-load transportation. *J. Hydraul. Div. ASCE*, 89:221–249.